

Supplementary Information for
Robust band gaps in the graphene/oxide heterostructure— SnO/graphene/SnO

Qing Guo[#], Gaoxue Wang[#], Ravindra Pandey[#] and Shashi P. Karna^{##}

[#]Department of Physics, Michigan Technological University, Houghton, Michigan 49931, USA

^{##}Weapons and Materials Research Directorate, U.S. Army Research Laboratory,
ATTN: RDRL-WM, Aberdeen Proving Ground,
Aberdeen, Maryland 21005-5069, United States

(June 6, 2018)

*Email: pandey@mtu.edu

S1: Brillouin zone of rectangular 12-atom unit cell

The position of the Dirac point depends on how we choose the shape or size of the supercell for calculations. In our work, we have used rectangular 12-atom unit cell for the SnO/graphene/SnO trilayer.

Figure S1 displays graphene's first Brillouin zone of the Wigner-Seitz 2-atom unit cell (shaded area), rectangular 4-atom unit cell (large black) and rectangular 12-atom unit cell (small red). As discussed in Suzuki's paper (2017, J of Modern Physics, 8, 607-621), the K and K' points of the Wigner-Seitz 2-atom unit cell are folded to Q and P points for the rectangular 4-atom unit cell. In our calculation, we used a unit cell 3 times of the 4-atom unit cell in Y direction (Figure S2(a)) which will reduce the b_2 vector to 1/3 in the reciprocal space while keeping b_1 vector the same (show in Figure S1(b), red rectangular). The P and Q-points of the rectangular 4-atom unit cell are now folded to Γ point, while the Y' point is folded to Y point, the W point is folded to S point and the X point remains the same.

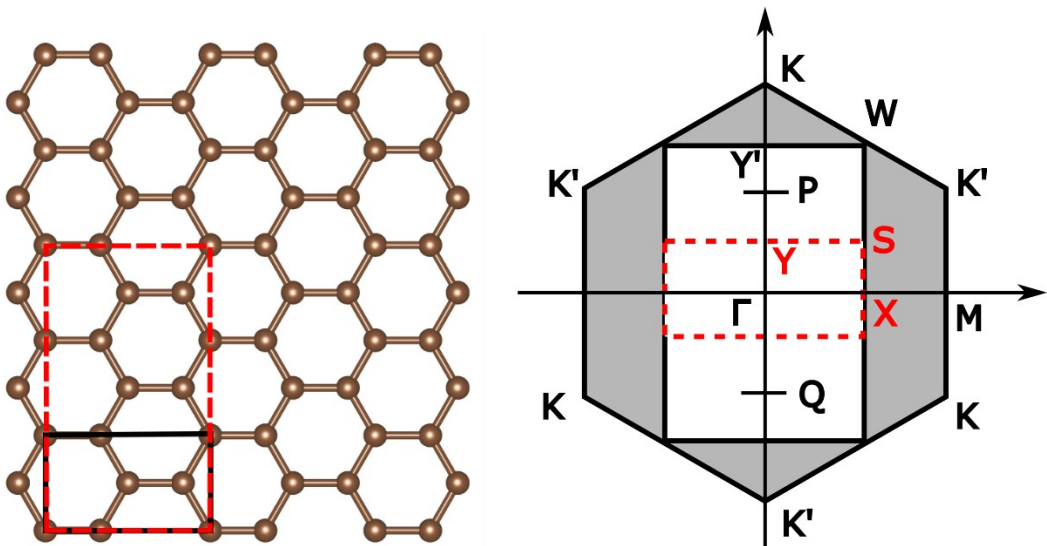


Figure S1 (a) The unit cell of graphene consisted of rectangular 4-atom unit cell (black line) and rectangular 12-atom unit cell (red dash line, this work) (b) The first Brillouin zone of the Wigner-Seitz 2-atom unit cell (shaded area), rectangular 4-atom unit cell (large black) [1]and rectangular 12-atom unit cell (small red). The high-symmetric points within the rectangular unit cell are indicated by, X, Y, W and S within the reciprocal lattice plane.

S2: Potential energy surface of the SnO/graphene/SnO

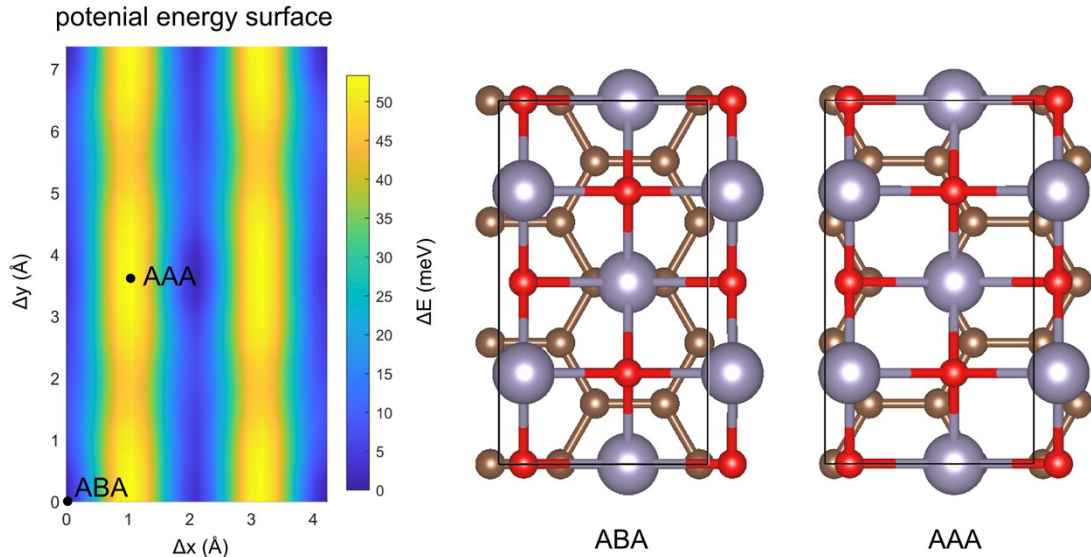


Figure S2. Calculated energy surface of shifting the graphene layer in the SnO/graphene/SnO trilayer configurations. Δx , Δy represent the displacement with respect to the ABA-stacked configuration.

S3. Charge density difference of ABA -stacked SnO/graphene/SnO tri-layer

The charge density difference is derived using the following formula:

$$\Delta \text{CHG} = \text{CHG_total} - (\text{CHG_topSnO} + \text{CHG_graphene} + \text{CHG_bottom_SnO}).$$

Here, “total” is the tri-layer structure, “top_SnO” is the top SnO monolayer, “graphene” is the middle layer and “bottom_SnO” indicates the bottom SnO monolayer.

The charge density difference is mainly due to the shape deformation of electron clouds which belong to different layers at the interface. Note that the contact in the trilayer configuration is a semiconductor-graphene contact. So, unlike the metal-graphene contact in the reference [2], there exists no extra unoccupied orbitals below the Fermi level of the heterostructure leading to absence of the p-doping at the interface.

Fig. S3 (b) shows the planar average charge density difference along the z-direction indicating occurrence of the charge space distribution variation compare

with the original SnO layers and graphene. A side- view of charge density difference plot in Fig. S3 (c) depicts this charge density difference in a more intuitive way: the blue regions around C atoms indicate reduction of electrons to the adjacent Sn atoms which are surrounded by the yellow regions. Asymmetry in the charge transfer is shown in the top view of charge density difference in Fig. S3 (c): a higher degree of the charge reduction around carbon atoms which are adjacent to Sn atoms with respect to carbon atoms which are far away from Sn atoms. This asymmetric charge distribution variation in the carbon sublattices introduces the finite band gap in graphene sandwiched between the oxide monolayers.

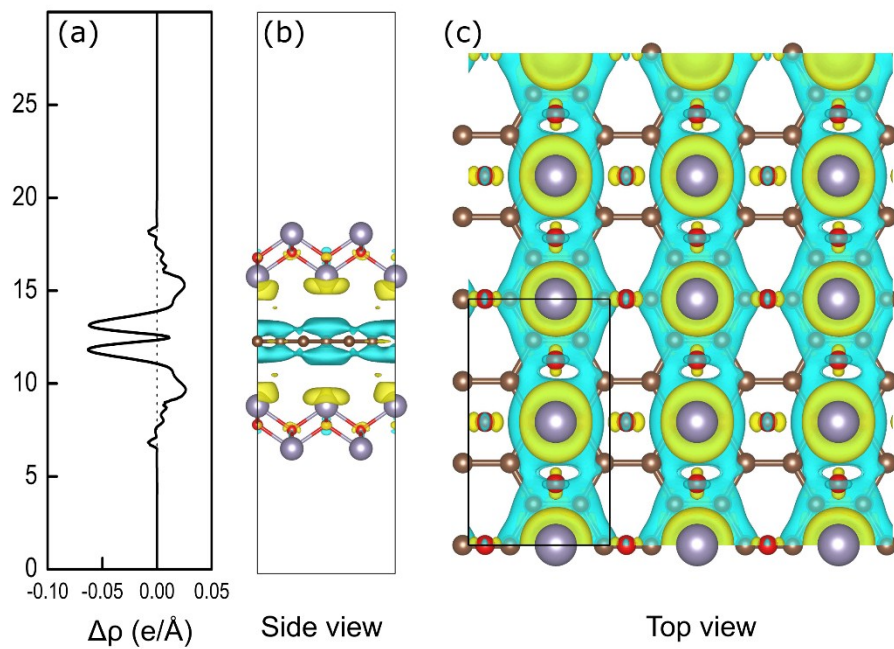


Figure S3. ABA-stacked SnO/graphene/SnO heterostructure: (a) The profile of the planar average charge density difference as a function of position along the z-direction. (b) side and (c) top views of the charge density difference with the isosurface value of $0.0014 \text{ e}/\text{\AA}^3$. The yellow and blue colors represent electron-rich and electron deficient regions, respectively. Color code: C: small brown sphere, Sn: large grey sphere and O: small red sphere.

S4. Comparison of results obtained using PBE-D2 and optB88-vdW functional forms

Note that both PBE-D2 and optB88-vdW level of theory provide similar results (Table S1). The band gap difference between the PBE-D2 and optB88-vdW functional forms comes out to be about 3~4 meV (Table S2). On the other hand, a larger gap is predicted for the HSE functional form, as expected.

Table S1 Total energy of SnO/graphene/SnO trilayer calculated using optB88-vdW and PBE-D2 functional forms.

Stacking Configuration	Relative Energy (eV)	
	PBE-D2	optB88-vdW
ABA	0	0
ABC	0.005	0.003
AAA	0.035	0.016

Table S2. Calculated band gaps of the ABA-stacked SnO/graphene/SnO tri-layer for the PBE-D2 optimized trilayer configuration.

Functional form	Band gap (eV)
PBE-D2	
optB88-vdW	0.115 eV
HSE06	0.111 eV
	0.240 eV

S5. Calculated band structures of SnO monolayer and SnO Bulk

The calculated band structure of a SnO monolayer is distinctly different from that of SnO bulk (Figure S4). A large direct band gap is predicted for SnO monolayer while a very small indirect band gap exists for SnO bulk [3, 4]. We also notice that the valence bands of SnO monolayer are much flatter than those of bulk SnO.

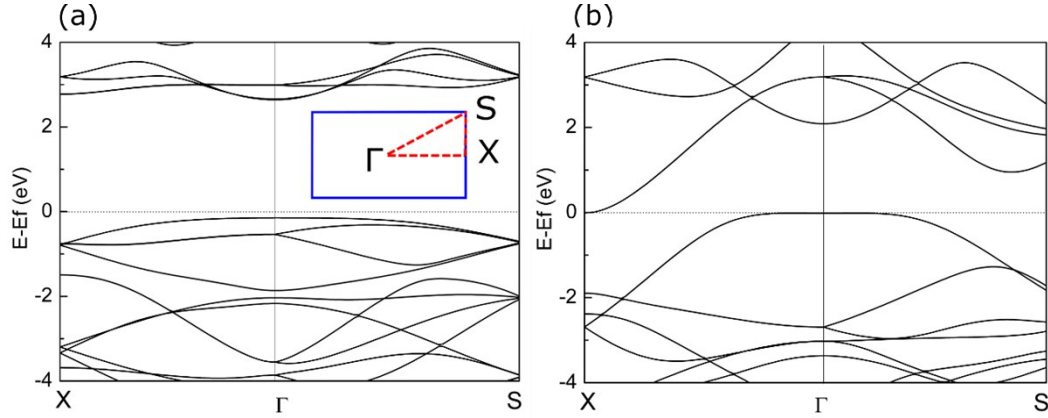


Figure S4: Calculated (PBE-D2) band structures of (a) SnO monolayer, and (b) SnO bulk.

S6. Multilayer heterostructures : ABAA- stacked SnO/graphene/SnO-bilayer and ABAAA-stacked SnO/graphene/SnO-trilayer heterostructures

As shown in Figure S5, top of the valence band associated with SnO layers has risen to the Fermi level with the increase of the substrate thickness. Consequently, the band gap is closed in graphene/oxide heterostructures with a thicker SnO substrate which will result in an Ohmic conductivity in the heterostructure.

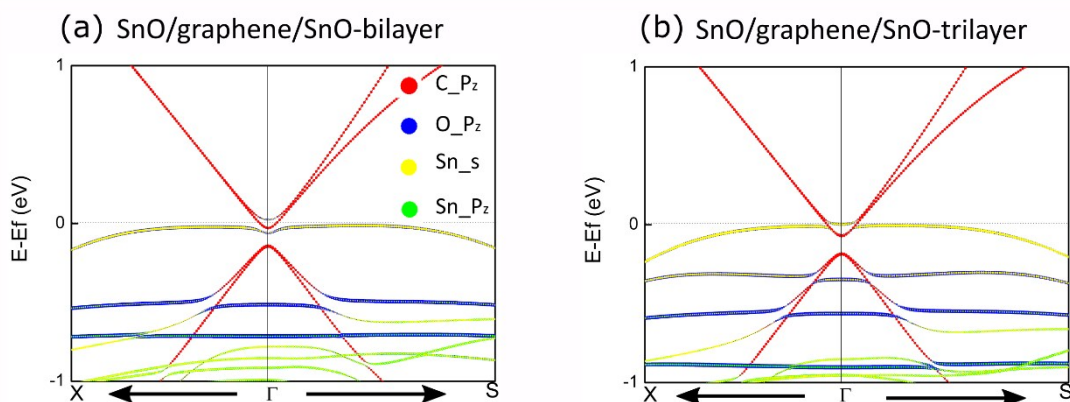


Figure S5: Calculated (PBE-D2) band structures of (a) ABAA SnO/graphene/SnO-bilayer and ABAAA SnO/graphene/SnO-trilayer heterostructures.

S7. Structure of the ABA and AAA stacked SnO/graphene/SnO trilayer

AAA.cif:

```
#=====
# CRYSTAL DATA
#-----
data_VESTA_phase_1

_pd_phase_name          'hetero'
_cell_length_a          4.23948
_cell_length_b          7.37038
_cell_length_c          30.00000
_cell_angle_alpha        90
_cell_angle_beta         90
_cell_angle_gamma        90
_symmetry_space_group_name_H-M   'P 1'
_symmetry_Int_Tables_number      1

loop_
_symmetry_equiv_pos_as_xyz
'x, y, z'

loop_
_atom_site_label
_atom_site_occupancy
_atom_site_fract_x
_atom_site_fract_y
_atom_site_fract_z
_atom_site_adp_type
_atom_site_B_iso_or_equiv
_atom_site_type_symbol
Sn1      1.0    0.618792    0.000190    0.298922    Bis0    1.000000 Sn
Sn2      1.0    0.119215    0.249696    0.222843    Bis0    1.000000 Sn
Sn3      1.0    0.618547    0.500202    0.298430    Bis0    1.000000 Sn
Sn4      1.0    0.119345    0.750700    0.222844    Bis0    1.000000 Sn
Sn5      1.0    0.617509    0.001034    0.529313    Bis0    1.000000 Sn
Sn6      1.0    0.116944    0.250309    0.605457    Bis0    1.000000 Sn
Sn7      1.0    0.617113    0.501053    0.529905    Bis0    1.000000 Sn
Sn8      1.0    0.116657    0.751763    0.605464    Bis0    1.000000 Sn
```

O1	1.0	0.118180	0.000221	0.265403	Biso	1.000000	O
O2	1.0	0.618204	0.249957	0.256335	Biso	1.000000	O
O3	1.0	0.118216	0.500223	0.265025	Biso	1.000000	O
O4	1.0	0.618234	0.750466	0.256337	Biso	1.000000	O
O5	1.0	0.116606	0.001026	0.562811	Biso	1.000000	O
O6	1.0	0.616504	0.250591	0.571955	Biso	1.000000	O
O7	1.0	0.116604	0.501023	0.563381	Biso	1.000000	O
O8	1.0	0.616459	0.751488	0.571978	Biso	1.000000	O
C1	1.0	0.209002	0.500151	0.413824	Biso	1.000000	C
C2	1.0	0.544077	0.500176	0.413844	Biso	1.000000	C
C3	1.0	0.709984	0.666563	0.413851	Biso	1.000000	C
C4	1.0	0.043050	0.666555	0.413851	Biso	1.000000	C
C5	1.0	0.210017	0.166334	0.413930	Biso	1.000000	C
C6	1.0	0.543017	0.166366	0.413933	Biso	1.000000	C
C7	1.0	0.709978	0.333780	0.413886	Biso	1.000000	C
C8	1.0	0.043006	0.333752	0.413878	Biso	1.000000	C
C9	1.0	0.210026	0.833984	0.413899	Biso	1.000000	C
C10	1.0	0.543037	0.833982	0.413902	Biso	1.000000	C
C11	1.0	0.708993	0.000174	0.413920	Biso	1.000000	C
C12	1.0	0.044096	0.000162	0.413918	Biso	1.000000	C

ABA.cif:

```
#=====
# CRYSTAL DATA
#
#-----
data_VESTA_phase_1

_pd_phase_name          'hetero'
_cell_length_a           4.23948
_cell_length_b           7.37038
_cell_length_c           30.00000
_cell_angle_alpha         90
_cell_angle_beta          90
_cell_angle_gamma         90
_symmetry_space_group_name_H-M   'P 1'
_symmetry_Int_Tables_number      1
```

```

loop_
_symmetry_equiv_pos_as_xyz
'x, y, z'

loop_
_atom_site_label
_atom_site_occupancy
_atom_site_fract_x
_atom_site_fract_y
_atom_site_fract_z
_atom_site_adp_type
_atom_site_B_iso_or_equiv
_atom_site_type_symbol

Sn1      1.0    0.618792    0.000190    0.298922    Bis0   1.000000 Sn
Sn2      1.0    0.119215    0.249696    0.222843    Bis0   1.000000 Sn
Sn3      1.0    0.618547    0.500202    0.298430    Bis0   1.000000 Sn
Sn4      1.0    0.119345    0.750700    0.222844    Bis0   1.000000 Sn
Sn5      1.0    0.617509    0.001034    0.529313    Bis0   1.000000 Sn
Sn6      1.0    0.116944    0.250309    0.605457    Bis0   1.000000 Sn
Sn7      1.0    0.617113    0.501053    0.529905    Bis0   1.000000 Sn
Sn8      1.0    0.116657    0.751763    0.605464    Bis0   1.000000 Sn
O1       1.0    0.118180    0.000221    0.265403    Bis0   1.000000 O
O2       1.0    0.618204    0.249957    0.256335    Bis0   1.000000 O
O3       1.0    0.118216    0.500223    0.265025    Bis0   1.000000 O
O4       1.0    0.618234    0.750466    0.256337    Bis0   1.000000 O
O5       1.0    0.116606    0.001026    0.562811    Bis0   1.000000 O
O6       1.0    0.616504    0.250591    0.571955    Bis0   1.000000 O
O7       1.0    0.116604    0.501023    0.563381    Bis0   1.000000 O
O8       1.0    0.616459    0.751488    0.571978    Bis0   1.000000 O
C1       1.0    0.959002    0.000151    0.413824    Bis0   1.000000 C
C2       1.0    0.294077    0.000176    0.413844    Bis0   1.000000 C
C3       1.0    0.459984    0.166563    0.413851    Bis0   1.000000 C
C4       1.0    0.793050    0.166555    0.413851    Bis0   1.000000 C
C5       1.0    0.960017    0.666334    0.413930    Bis0   1.000000 C
C6       1.0    0.293017    0.666366    0.413933    Bis0   1.000000 C
C7       1.0    0.459978    0.833780    0.413886    Bis0   1.000000 C
C8       1.0    0.793006    0.833752    0.413878    Bis0   1.000000 C
C9       1.0    0.960026    0.333984    0.413899    Bis0   1.000000 C
C10      1.0    0.293037    0.333982    0.413902    Bis0   1.000000 C
C11      1.0    0.458993    0.500174    0.413920    Bis0   1.000000 C
C12      1.0    0.794096    0.500162    0.413918    Bis0   1.000000 C

```

References

1. Suzuki, A., M. Tanabe, and S. Fujita, *Electronic Band Structure of Graphene Based on the Rectangular 4-Atom Unit Cell*. Journal of Modern Physics, 2017. **8**(04): p. 607.
2. Dedkov, Y. and E. Voloshina, *Graphene growth and properties on metal substrates*. Journal of Physics: Condensed Matter, 2015. **27**(30): p. 303002.
3. Zhou, W. and N. Umezawa, *Band gap engineering of bulk and nanosheet SnO: an insight into the interlayer Sn-Sn lone pair interactions*. Phys Chem Chem Phys, 2015. **17**(27): p. 17816-20.
4. Du, J., et al., *Electronic characteristics of p-type transparent SnO monolayer with high carrier mobility*. Applied Surface Science, 2017. **401**: p. 114-119.